Iridium Metal Complexes Containing N-heterocyclic Carbene Ligands for Blue Light-Emitting Electrochemical Cells

Journal:	*Inorganic Chemistry*
Manuscript ID:	ic-2010-009253.R2
Manuscript Type:	Article
Date Submitted by the Author:	10-Sep-2010
Complete List of Authors:	De Cola, Luisa; Westfaelische Wilhelms-Universitaet, Physikalisches Institut

Iridium Metal Complexes Containing N-heterocyclic Carbene Ligands for Blue Light-Emitting Electrochemical Cells

Cheng-Han Yang, [1]Juan Beltran,[2] Vincent Lemaur,[2] Jérôme Cornil,[2]David Hartmann, [3] Wiebke Sarfert, [3] Roland Fröhlich[4], Claudia Bizzarri, [1]and Luisa De Cola[1]*

[1]Westfälische Wilhelms-Universität Münster, Physikalisches Institut, Mendelstrasse 7, 48149 Münster, Germany; and Center for Nanotechnology (CeNTech), Heisenbergstrasse 11, 48149 Münster, Germany.

[2]Université de Mons, Service de Chimie des Matériaux Nouveaux, Place du Parc 20, 7000 Mons, Belgium.

[3]Siemens AG, Corporate Technology, CT MM 1, Günther-Scharowsky Strasse 1, 91058 Erlangen, Germany

[4] Westphälische Wilhelms-Universität Münster, Organisch-Chemisches Institut, Corrensstrasse 40, 48149 Münster, Germany

decola@uni-muenster.de

RECEIVED DATE (to be automatically inserted after your manuscript is accepted if required according to the journal that you are submitting your paper to)

Abstract

A new series of cationic blue-emitting, heteroleptic Ir(III) based metal complexes were systematically synthesized using two 4,6-difluorophenyl pyridine as well as one methyl or *n*-butyl substituted bisimidazolium salt carbene-type ligands. In degassed CH_2Cl_2, all complexes display highly efficient, blue phosphorescence (λ_{max} ~ 452 nm, quantum yield ~ 0.30) at room temperature and also show blue emission in thin film. The measured photophysical properties of the complexes have been rationalized with the help of quantum-chemical calculations. Due to the high solubility of the complexes, solution processed devices, light-emitting electrochemical cells (LEECs), based on **2a** and **2b** were made. The results showed that true-blue emission and short turn on time is achieved when an ionic conductor, tetrabutylammonium trifluoromethanesulfonate was used as matrix for the film containing the emitters. These iridium complexes and the described devices are the bluest materials ever reported and the first case of LEECs based on carbene ligands.

Keywords:, Iridium, Blue-light-emitting, Light-emitting electrochemical cells, TD-DFT calculations, singlet and triplet excited states.

Introduction

Recently, electroluminescent devices, Light-Emitting Electrochemical Cells (LEECs), based on ionic transition metal complexes (iTMCs) have been subject of many investigations for their simplest structure and ease of manufacturing with respect to the organic light emitting diode, OLED, preparation. [1] In such simple devices, the electroluminescent layer, which is ionic in nature is deposited by solution processing techniques, and due to the presence of mobile ions, that redistribute under an applied field and assist charge injection, the working mechanism of the device relies on ionic transport, differently from the OLEDs. In particular upon application of an external bias, in the LEECs, ions in the single active layer migrate and accumulate at the electrode interfaces, leading to a strong interfacial electrical field that greatly facilitates the injection of electrons and holes. [2] Most of the iTMCs materials reported in the literature are based on ruthenium[3], osmium[4], copper[5] and iridium[6,7,8] complexes and typically they emit in the red, orange, yellow, green and sky blue region. Among these complexes, iridium complexes are interesting candidates in terms of the color tuning due to the pronounced ligand-field splitting effects. Recently, *Wong* and *Qiu* et al. reported the white LEECs base on cationic iridium complexes. [9] However, reports concerning the design and preparation of blue or even near-UV ionic phosphorescent materials also based on other metal ions, are relatively rare.[10]

In particular, amongst the Ir(III) complexes, a great number of ancillary ligands (*e.q.*, picolate, pyrazolylborate and pyridyl azolate based ligands) have been explored in order to obtain blue emission for application as OLEDs materials.[11] Despite a lot of efforts, experimental and theoretical studies have pointed out the intrinsic difficulties in obtaining deep blue emission, since increasing the HOMO-LUMO energy gap induces a destabilization of the MLCT state and hence a decrease in the MLCT character of the lowest luminescent triplet excited state. This implies that the excited state becomes more ligand centered, with a stronger coupling to the intramolecular vibrational modes, and that the oscillator strength of the S_0-T_1 transition is reduced as well as the emission quantum efficiency, while the radiative lifetime is increased. It has been recently reported that the use of high-field strength ligands such as carbenes results in a shift towards higher energy of the emission, and an increase of the

blue phosphorescent efficiency.[12] The number of papers exploiting carbene as high-field ligand however remains scarce though such ligands appear as good candidates to achieve high performing OLED displays, and to the best of our knowledge no reports on LEEC devices have been published.

Herein, we report a new strategy to synthesize cationic blue-emitting, heteroleptic Ir(III)-based phosphors employing methyl or *n*-butyl substituted bisimidazolium salt N-heterocyclic carbene ligands as the ancillary chelate of a dfppy (4,6-difluorophenyl pyridine) Ir(III) complex. A full photophysical and electrochemical characterization has been performed and the experimental results compared and rationalized with quantum-chemical calculations. These complexes display deep blue emission and high luminescent quantum yields and due to their excellent solubility in organic solvents have been employed as blue phosphors to fabricate blue-emitting LEECs. The emission wavelengths of the devices obtained are still very blue, the bluest ever reported for cationic species, and the LEECs possess fast turn-on time.

Experimental

General Information and Materials. The methyl and n-butyl substituted bisimidazolium salts (**L1** and **L2**) were prepared from the reaction of 1-methylimidazole, 1-n-butylimidazole and diiodomethane in THF.[10b] The iridium complex $[(dfppy)_2Ir(\mu\text{-}Cl)]_2$ was synthesized using $IrCl_3 \cdot nH_2O$ and 4,6-difluorophenyl pyridine (dfppy) in 2-ethoxyethanol according to literature method.[13] The solvents were dried using standard procedures. All other reagents were used as received from commercial sources, unless otherwise stated. NMR spectra were recorded on an ARX 300 or an AMX 400 from Bruker Analytische Messtechnik (Karlsruhe, Germany). The ^1H NMR chemical shifts (δ) of the signals are given in ppm and referenced to residual protons in the deuterated solvents: chloroform-d_1 (7.26 ppm), dimethyl sulfoxide-d_6 (2.50 ppm), or acetone-d_6 (2.09 ppm). The ^{19}F NMR chemical shifts are referenced to $CFCl_3$ (0.00 ppm) as an internal standard. The signal splittings are abbreviated as follows: s = singlet; d = doublet; t = triplet; q = quartet; m = multiplet. All coupling constants (*J*) are given in Hertz (Hz). Mass spectrometry was performed in the Department of Chemistry, University of Münster.

Electrospray ionization (ESI) mass spectra were recorded on a Bruker Daltonics (Bremen, Germany) MicroTof with loop injection. Elemental analysis was recorded at the University of Milan, Italy.

Preparation of 1,1'-dimethyl-3,3'-methylene-diimidazolium diiodide. **(L1)**

A mixture of 1-methylimidazole (12 mmol, 1.0 g, 0.97 mL) and diiodomethane (6 mmol, 1.61 g, 0.5 mL) were dissolved in 2 mL tetrahydrofuran in a pressure tube. The reaction mixture was stirred for 1h at 110 °C until a white precipitate was formed. The solid was filtered off and washed with tetrahydrofuran (5 mL) and toluene (5 mL). After that the product was dried in vacuo and obtained as a white powder (2.31 g, 5.3 mol, 89 %).

Spectra: ^{1}H NMR (300 MHz, DMSO): δ 9.40 (s, 1H), 7.99 (t, *J* = 1.8, 1H), 7.81 (t, *J* = 1.8, 1H), 6.67 (s, 1H), 3.90 (s, 3H). Anal. Calcd for $C_9H_{14}I_2N_4$: C, 25.02; H, 3.27; N, 12.97. Found: C, 25.11; H, 3.32; N, 12.84 %.

Preparation of 1,1'-di-*n*-butyl-3,3'-methylene-diimidazolium diiodide **(L2)**

A mixture of 1-*n*-butylimidazole (7.6 mmol, 0.945 g, 1.0 mL) and diiodomethane (3.8 mol, 1.013 g, 0.30 mL) were dissolved in 2 mL tetrahydrofuran in a sealed tube. The reaction mixture was stirred for 3 h at 110 °C until a white precipitate was formed. The solid was filtered off and washed with tetrahydrofuran (5 mL) and toluene (5 mL). After that the product was dried in vacuo and obtained as a white powder (3.22 g, 6.2 mmol, 82 %).

Spectra: ^{1}H NMR (300 MHz, DMSO) δ 9.47 (s, 1H), 8.01 (t, *J* = 1.7, 1H), 7.92 (t, *J* = 1.8, 1H), 6.64 (s, 1H), 4.23 (t, *J* = 7.2, 2H), 2.00 – 1.66 (m, 2H), 1.29 (dq, *J* = 7.3, 14.6, 2H), 0.90 (t, *J* = 7.3, 3H). Anal. Calcd for $C_{15}H_{26}I_2N_4$: C, 34.90; H, 5.08; N, 10.85. Found: C, 34.72; H, 4.94; N, 10.92 %.

Preparation of 1a: Bis[2-(4,6-difluorophenyl)pyridinato-N,C^2]iridium(III)[1,1'-dimethyl-3,3'-methylene-diimidazoline-2,2'-diylidene] hexafluorophosphate

A mixture of 1,1'-dimethyl-3,3'-methylene-diimidazolium diiodide (0.036 g, 0.083 mmol), Ag_2O (0.04 g, 0.17 mmol) and the dichloro-bridged cyclometalated iridium complex $[(dfppy)_2Ir(\mu\text{-}Cl)]_2$ (0.05 g, 0.04 mmol) in 2-ethoxyethanol (10 mL) was heated to reflux for 12 hours in the dark. After cooling to room temperature, the solution was filtered through a sintered glass-fritted and an excess (10 eq) of NH_4PF_6 (in 20 mL H_2O) was added to induce the precipitation. The yellow precipitate was collected by filtration and washed with excess H_2O then dried under vacuum. The solid was separated using silica gel column chromatography (CH_2Cl_2 : MeCN = 9 : 1), giving a light-yellow complex **1a** (0.052 g, 0.058 mmol, 72 % yield).

Spectra: ^{1}H NMR (300 MHz, Acetone) δ 8.55 (dd, *J* = 0.8, 5.9, 1H), 8.41 (d, *J* = 8.6, 1H), 8.10 (ddd, *J* = 0.5, 4.5, 8.3, 1H), 7.56 (d, *J* = 1.9, 1H), 7.30 (ddd, *J* = 1.4, 5.9, 7.3, 1H), 7.25 (d, *J* = 1.9, 1H), 6.58 (ddd, *J* = 2.4, 9.2, 12.9, 1H), 6.39 (s, 1H), 5.92 (dd, *J* = 2.4, 8.5, 1H), 3.01 (s, 3H). ^{19}F–{^{1}H} NMR (282 MHz, Acetone,): δ -71.25 (3F), -73.75 (3F), -109.68 (2F), -110.48 (2F). ^{13}C NMR (101 MHz, DMSO) δ 168.36, 164.50, 163.22, 162.18, 160.72, 159.76, 159.47, 153.72, 138.87, 127.95, 124.30, 123.19, 121.95, 112.77, 97.86, 61.63, 36.47. HRMS found 749.1613 ($[M - PF_6]^+$). Anal. Calcd for $C_{31}H_{24}F_{10}IrN_6P$: C, 41.66; H, 2.71; N, 9.40. Found: C, 41.53; H, 2.84;N, 9.46 %.

Preparation of 1b: Bis[2-(4,6-difluorophenyl)pyridinato-N,C^2]iridium(III)[1,1'-dimethyl-3,3'-methylene-diimidazoline-2,2'-diylidene] tetrafluoroborate

A mixture of 1,1'-dimethyl-3,3'-methylene-diimidazolium diiodide (0.36 g, 0.83 mmol), Ag_2O (0.4 g, 1.7 mmol) and the dichloro-bridged cyclometalated iridium complex $[(dfppy)_2Ir(\mu\text{-}Cl)]_2$ (0.5 g, 0.4 mmol) in 2-ethoxyethanol (20 mL) was heated to reflux for 12 hours in the dark. After cooling to room temperature, the solution was then filtered through a sintered glass-fritted and an excess (10 eq) of $NaBF_4$ (in 40 mL H_2O) was added to induce the precipitation. The yellow precipitate was collected by filtration and washed with H_2O then dried under vacuum. The solid was separated using silica gel column chromatography (CH_2Cl_2 : MeCN = 9 : 1), giving a light-yellow complex **1b** (0.46 g, 0.56 mmol, 68 % yield).

Spectra: ^{1}H NMR (300 MHz, Acetone) δ 8.60 – 8.51 (m, 1H), 8.46 – 8.35 (m, 1H), 8.16 – 8.03 (m, 1H), 7.58 (d, *J* = 2.0, 1H), 7.31 (ddd, *J* = 1.4, 5.9, 7.4, 1H), 7.23 (d, *J* = 2.0, 1H), 6.57 (ddd, *J* = 2.4, 9.2, 12.9, 1H), 6.38 (s, 1H), 5.92 (dd, *J* = 2.4, 8.5, 1H), 3.00 (s, 3H). ^{19}F–{^{1}H} NMR (282 MHz, Acetone,): δ -109.80 (2F), -110.52 (2F), -151.06 (4F). ^{13}C NMR (101 MHz, DMSO) δ 168.29, 164.42, 163.19, 162.14, 160.62, 159.64, 159.15, 153.66, 138.91, 128.16, 124.18, 123.20, 121.94, 112.57, 97.78, 61.64, 36.63. HRMS found 749.1635 ([M – BF_4]$^+$). Anal. Calcd for $C_{31}H_{24}BF_8IrN_6$: C, 44.56; H, 2.90; N, 10.06. Found: C, 44.09; H, 2.92; N, 9.84 %.

Preparation of 2a: Bis[2-(4,6-difluorophenyl)pyridinato-N,C^2]iridium(III)[1,1'-di-n-butyl-3,3'-methylene-diimidazoline-2,2'-diylidene] hexafluorophosphate

A mixture of 1,1'-di-*n*-butyl-3,3'-methylene-diimidazolium diiodide (0.045 g, 0.087 mmol), Ag_2O (0.04 g, 0.17 mmol) and the dichloro-bridged cyclometalated iridium complex $[(dfppy)_2Ir(\mu\text{-}Cl)]_2$ (0.05 g, 0.04 mmol) in 2-ethoxyethanol (10 mL) was heated to reflux for 12 hours in the dark. After cooling to room temperature, the solution was filtered through a sintered glass-fritted and an excess (10 eq) of NH_4PF_6(in 20 mL H_2O) was added to induce the precipitation. The yellow precipitate was collected by filtration and washed with H_2O then dried under vacuum. The solid was separated using silica gel column chromatography (CH_2Cl_2 : MeCN = 9 : 1), giving a light-yellow complex **2a** (0.056 g, 0.057 mmol, 79 % yield).

Spectra: ^{1}H NMR (300 MHz, Acetone) δ 8.51 (dd, *J* = 0.8, 5.9, 1H), 8.48 – 8.40 (m, 1H), 8.11 (ddd, *J* = 0.9, 7.5, 8.3, 1H), 7.61 (d, *J* = 2.0, 1H), 7.39 – 7.29 (m, 2H), 6.60 (ddd, *J* = 2.4, 9.2, 12.9, 1H), 6.35 (s, 1H), 5.87 (dd, *J* = 2.4, 8.5, 1H), 3.59 – 3.33 (m, 2H), 1.29 – 1.09 (m, 1H), 0.94 – 0.74 (m, 2H), 0.65 (t, *J* = 7.2, 3H), 0.52 – 0.30 (m, 1H). ^{19}F–{^{1}H} NMR (282 MHz, Acetone,): δ -71.16 (3F), -73.66 (3F), -109.20 (2F), -110.38 (2F). ^{13}C NMR (101 MHz, DMSO) δ 168.18, 164.45, 163.56, 162.24, 161.14, 159.53, 159.28, 153.85, 138.90, 128.18, 124.55, 123.53, 123.14, 122.98, 112.24, 97.64, 62.02, 48.61, 32.78, 19.42, 13.68. HRMS found 833.2576 ([M – PF_6]$^+$). Anal. Calcd for $C_{37}H_{36}F_{10}IrN_6P$: C, 45.44; H, 3.71; N, 8.59. Found: C, 45.04; H, 3.62; N, 8.41 %.

Preparation of 2b: Bis[2-(4,6-difluorophenyl)pyridinato-N,C^2]iridium(III)[1,1'-di-n-butyl-3,3'-methylene-diimidazoline-2,2'-diylidene] tetrafluoroborate

A mixture of 1,1'-di-*n*-butyl-3,3'-methylene-diimidazolium diiodide (0.045 g, 0.087 mmol), Ag_2O (0.04 g, 0.17 mmol) and the dichloro-bridged cyclometalated iridium complex $[(dfppy)_2Ir(\mu\text{-}Cl)]_2$ (0.05 g, 0.04 mmol) in 2-ethoxyethanol (10 mL) was heated to reflux for 12 hours in the dark. After cooling to room temperature, the solution was filtered through a sintered glass-fritted and an excess (10 eq) of $NaBF_4$ (in 20 mL H_2O) was added to induce the precipitation. The yellow precipitate was collected by filtration and washed with H_2O, then dried under vacuum. The solid was separated using silica gel column chromatography (CH_2Cl_2 : MeCN = 9 : 1), giving a light-yellow complex **2b** (0.055 g, 0.059 mmol, 74 % yield)

Spectra: ^{1}H NMR (300 MHz, Acetone) δ 8.52 (dd, *J* = 0.8, 5.9, 1H), 8.43 (d, *J* = 8.7, 1H), 8.11 (dd, *J* = 7.7, 8.5, 1H), 7.64 (d, *J* = 2.0, 1H), 7.39 – 7.26 (m, 2H), 6.60 (ddd, *J* = 2.4, 9.2, 12.9, 1H), 6.34 (s, 1H), 5.87 (dd, *J* = 2.4, 8.5, 1H), 3.58 – 3.35 (m, 2H), 1.19 (td, *J* = 5.8, 10.9, 1H), 0.96 – 0.72 (m, 2H), 0.65 (t, *J* = 7.2, 3H), 0.53 – 0.27 (m, 1H). ^{19}F–{^{1}H} NMR (282 MHz, Acetone,): δ -109.27 (2F), -110.44 (2F), -151.04 (4F). ^{13}C NMR (101 MHz, DMSO) δ 168.16, 164.36, 163.55, 162.30, 160.85, 159.64, 159.13, 153.76, 138.92, 128.06, 124.20, 123.52, 122.80, 122.44, 112.12, 97.48, 61.77, 48.55, 32.63, 19.27, 13.19. HRMS found 833.2558 ([M – BF_4]$^+$). Anal. Calcd for $C_{37}H_{36}BF_8IrN_6$: C, 48.32; H, 3.95; N, 9.14. Found: C, 48.01; H, 4.03; N, 9.05 %.

Photophysics

Absorption spectra were measured on a Varian Cary 5000 double-beam UV-Vis-NIR spectrometer and baseline corrected. Steady-state emission spectra were recorded on a HORIBA Jobin-Yvon IBH FL-322 Fluorolog 3 spectrometer equipped with a 450 W xenon arc lamp, double grating excitation and emission monochromators (2.1 nm mm dispersion^{-1}; 1200 grooves mm^{-1}) and a Hamamatsu R928 photomultiplier tube or a TBX-4-X single-photon-counting detector. Emission and excitation spectra were corrected for source intensity (lamp and grating) and emission spectral response (detector and

grating) by standard correction curves. Time-resolved measurements were performed using the time-correlated single-photon counting (TCSPC) option on the Fluorolog 3. NanoLEDs (295, 402 and 431 nm; FWHM < 750 ps) with repetition rates between 10 kHz and 1 MHz were used to excite the sample. The excitation sources were mounted directly on the sample chamber at 90^{o} to a double grating emission monochromator (2.1 nm mm^{-1} dispersion; 1200 grooves mm^{-1}) and collected by a TBX-4-X single-photon-counting detector. The photons collected at the detector are correlated by a time-to-amplitude converter (TAC) to the excitation pulse. Signals were collected using an IBH DataStation Hub photon counting module and data analysis was performed using the commercially available DAS6 software (HORIBA Jobin Yvon IBH). The quality of the fit was assessed by minimizing the reduced chi-squared function (χ^2) and visual inspection of the weighted residuals. The quantum yield measurements were performed in a deaerated dichloromethane solution at 300 nm of excitation wavelength using the absolute quantum yield measurement system from Hamamatsu, model C9920-01.

X-Ray crystallography.

Data sets were collected with a Nonius KappaCCD diffractometer, equipped with a rotating anode generator. Programs used: data collection COLLECT,[14] data reduction Denzo-SMN,[15] absorption correction SORTAV[16,17] and Denzo,[18] structure solution SHELXS-97,[19] structure refinement SHELXL-97,[20] graphics SCHAKAL.[21] The crystallographic refinement parameters of complexes **1a** and **2a** are summarized in Table S1, and Figure S1 shows the crystal structure of complex **1a**.

Cyclic voltammetry.

Cyclic voltammetry (CV) was performed using a CH instrument workstation from CH instrument which consists of a CH750 potentiostat and software. The working and the counter electrodes were a Pt disc and a Pt wire respectively, whereas Ag wire was used as a pseudoreference electrode. All glassware was dried prior to use. The dry electrolyte tetrabutylammonium perchlorate (>99.0% purity) was used after recrystallization. The analyte and ferrocene ($FeCp_2$) used as the reference were dried and degassed at high temperature and at reduced pressure in a Schlenk flask in order to eliminate any moisture and

oxygen. The flask was then evacuated and filled three times with N_2 flow. Acetonitrile freshly distilled from P_2O_5 was added via syringe directly into the sealed Schlenk flask, the solution sonicated if necessary and then degassed for ten minutes with a gentle stream of nitrogen. The degassed solution was injected into the electrochemical cell and, after the introduction of electrodes, measurements were done under nitrogen atmosphere.

Computational Method:

The ground-state geometry of the complexes **1a** and **2a** has been optimized at the density functional theory (DFT) level, starting from the X-ray structures and from the measured distance between the Ir center and the P atom of the $PF6^-$ counter-ion. The chosen exchange correlation (XC) functional is the widely used B3LYP[22] in view of its good compromise between accuracy and computational cost; the basis set for the description of the electrons of non-metallic atoms is 6-31G**[23] while the LANL2DZ basis set has been used for Ir.[24] The characterization of the nature of the lowest-lying singlet and triplet excited states relies on time-dependent density functional theory (TD-DFT) calculations performed on the basis of the ground-state geometry, using the same functional and basis set. This choice is motivated by previous works showing the adequacy of this approach to describe the electronic and optical properties of iridium complexes[25] and of other complexes.[26] Note that these calculations neglect intersystem crossing processes mixing states of the singlet and triplet manifold. All calculations were performed with the Gaussian03 code.[27]

Fabrication of Light-Emitting Devices.

All devices had an active area of 4 mm² and were fabricated by spin-coating on indium tin oxide (ITO) coated glass substrates. The device structure consists of 100 nm poly(3,4-ethylenedioxythiophene): poly(styrenesulfonate) (PEDOT:PSS) and 70 nm of emitting layer composed of iTMC blended with TBAOTf (Tetrabutylammonium trifluoromethanesulfonate) as ionic conductor. The PEDOT:PSS (Clevios AI4083) was supplied by H. C. Starck and the TBAOTf from Sigma

Aldrich. The emitting layer solution was prepared in the following way: 10 mg of the transition metal complex material together with the ionic conductor was diluted in 1mL acetonitrile in a mole ratio 1:1. Before spin coating the solution was filtered using a 0.1µm PTFE-filter. The wet film was baked for 2 hours at 80°C in a vacuum oven. Finally, a 150-200 nm thick Al-cathode was evaporated on top followed by an encapsulation to protect the organic layers from oxygen and water. All electrical characterizations of the LEECs were performed using a power source-meter E3646A from Agilent Technologies. The resulting light output was detected by photo-diodes. The induced current through the device and through the photo-diodes were measured by current meters from National Instruments (NI9219). The current compliance for device current was set to 40mV. Using a spectral camera (PR650) the photodiode current was calibrated and the electroluminescent spectrum of the different LEECs devices was detected in the visible range between 380 and 780 nm.

Result and Discussion

Synthesis and X-ray Structure Characterization.

A synthetic pathway leading to the desired Ir(III) complexes is depicted in Scheme 1**.** The targeted complexes were synthesized by a combination of iridium dimer complex $[(dfppy)_2Ir(\mu\text{-}Cl)]_2$ with a stoichiometric amount of methyl or n-butyl substituted bisimidazolium salts and Ag_2O in 2-ethoxyethanol, to promote the chloride removal, followed by replacement of the Cl^- with PF_6^- or BF_4^-. The complexes were synthesized containing the *n*-butyl group as substituent of the carbene ligand, are useful to increase the solubility of the complex in common organic solvents.

After purification and recrystallization of the complexes detailed characterizations were carried out using high resolution MS, ^1H, ^{13}C and ^{19}F NMR spectroscopy, and elemental analysis (see experimental section for details).

Crystals of **1a** and **2a,** suitable for the X-ray diffraction analysis were obtained by slow evaporation of diethyl ether into an acetonitrile solution. Table 1 reports selected bond lengths and angles for the

structures. As depicted in Figure 1, complex **2a** exhibit a distorted octahedral geometry around the Ir atom coordinated to two cyclometalated dfppy ligands and one symmetrical biscarbene ligand. The dfppy ligands adopt a mutually eclipsed configuration with the nitrogen atoms N(21) and N(41) residing at the trans locations with distances Ir-N(21) = 2.055(1) and Ir-N(41) = 2.072(1) Å. The substituted phenyl groups are arranged *cis* to each other with the distances Ir-C(32)= 2.054(1) and Ir-C(52) = 2.054(1) Å. Moreover, the overall structural arrangement is similar when compared to several previously reported examples. [28] The pertinent bond angles and distances around iridium are identical within their estimated standard deviation, indicating that the peripheral methyl and *n*-butyl substituents have no significant stereo electronic effects on the metal center. The carbene bite angle C(1)-Ir-C(11) (**1a**) and C(2)- Ir-C(12) (**2a**) of 85.82(18)° and 85.28(15)° are very appropriate for octahedral coordination. To the best of our knowledge this is the first structure of bis-imidazolium carbene ligand bound to phenylpyridine complex.

We have first validated our theoretical approach by comparing the representative distance and bond angle of the DFT-optimized geometries to the corresponding experimental values. This information is included in Table S2 in the supporting information.

The calculated and experimental geometric parameters are in very good agreement, with differences systematically below 3 %. The best match is found for the Ir-C(dfppy) distance and for the angle values while the Ir-C(carbene) distances differ typically by 2-3% compared to the experimental values. This agreement ensures a proper description of the nature of the lowest excited states, provided that the complex keeps a similar geometry in solution.

There is a larger discrepancy when comparing the distance between the Ir atom in the complex and the phosphorus atom in the counter-ion (Ir-P=7.137 Å in the X-ray structure versus Ir-P=6.284 Å at the theoretical level, see Figure 2). This can be intuitively understood by the fact that the location of the counter-ion is more flexible in the gas phase (or in solution) compared to the solid state. The geometric parameters are found to be weakly affected when the counter-ion is not included, thus showing the weak impact of the electrostatic interactions on the molecular geometry. On the other hand, the counter-ion

has a strong impact on the electronic structure of the complexes; this is illustrated in Table S3 in the supporting information, showing the contribution of the different fragments (Ir, carbene ligand, dfppy1 and dfppy2, and counter-ion) to the frontier electronic levels of complex **1a** as well as the energies of these levels from calculations performed with and without the counter-ion. Similar trends are observed for complex **2a**. These results indicate that the counter-ion does not participate to the description of the frontier electronic levels; however, the electrostatic interactions induced by the counter-ion are found to significantly shift the energies of the one-electron levels, to modulate for some their fragment contributions and to break the symmetry of the orbitals localized on the individual ligands (when the counter-ion is not positioned symmetrically with respect to the ligand). The electronic structure of the complexes and their optical properties are discussed hereafter on the basis of the optimized ground-state geometry in the presence of the counter-ion. The most stable geometry of the system has been first determined by running geometry optimizations from starting geometries featuring different locations of the counterion.

Electronic structure

We have first examined the nature of the frontier electronic levels that will be predominantly involved in the lowest excited states of the complexes, by analyzing for each electronic level the contribution of the different fragments. Table 2 collects the energies of the frontier electronic levels of complexes **1a** and **2a** as well as the contribution of the different fragments.

The contributions of the different fragments in the HOMO and LUMO are similar for both complexes. The HOMO level has a strong weight on Ir while the LUMO is essentially localized on dfppy2. However, the occupied levels become already different for the HOMO-1 level, which has its largest contribution from Ir in **2a** and from dfppy1 for **1a**. Actually, the HOMO-1 level of **2a** appears to be very similar to the HOMO-2 of **1a,** thus pointing to changes in the ordering of the states between the two complexes as expected from their small energy separation. This one-to-one correspondence is extended down to the HOMO-5 orbital. On the other hand, the nature of the lowest unoccupied levels is very

similar in the two complexes up to the LUMO+4 level. We go next deeper into the analysis of the electronic structure of complex **1a**. The electronic structure and shape of the frontier electronic levels of this complex is graphically displayed in Figure 3.

The contribution of the carbene ligand is small for the orbitals ranging from HOMO-5 to LUMO+3 while reaching typical values larger than 35% in deeper levels. The two phenyl-pyridine moieties are alternatively the most contributing ligand going from LUMO to LUMO+3. These two ligands are thus expected to be strongly involved in the description of the low-lying excited states. Moreover, they contribute to most of the orbitals by more than 20% so that many excited states should be described by a mixture of different transition characters. In both complexes, the largest electronic density in the HOMO is supported by the phenyl ring of dfppy while the LUMO is mostly centered on the pyridine ring, as expected from the larger electronegativity of the nitrogen atom. When increasing the size of the alkyl chain, going from **1a** to **2a,** the order of the highest occupied levels is reversed while other electronic levels experience an energy shift; on the other hand, the electronic bandgap is found to be very similar for both complexes.

Photophysical Properties

Figure 4 shows the UV/Vis absorption and emission spectra of complexes **1** and **2** in CH_2Cl_2 solutions. In general, the dominant absorption band in the spectral region ≤ 300 nm is attributed to the spin allowed $^1\pi\pi^*$ transition characteristic of the ligands. The structureless band at ~ 300 – 360 nm for **1** and **2** is likely to result from a combination of substituted phenyl-to-pyridine inter-ligand $\pi\pi^*$ transition (LLCT) with Ir(d_π) to phenylpyridyl ligand transition (MLCT) in the singlet manifold. The lowest–lying bands that appear in the region > 360 nm are assigned to singlet and triplet MLCT transitions which however have a strong $\pi\pi*$ transition character. In this context, we have calculated the nature of lowest singlet excited states at the TD-DFT level strongly coupled to the singlet ground state to assist the interpretation of the experimental spectra.

Table 3 reports the calculated energies of the excited states with the largest oscillator strengths together with the nature of the dominant one-electron-transition. The theoretical results reproduce very well the three energy ranges observed in the experimental spectra, yielding the most intense band located around 250 nm, the second one around 300 nm and a less intense peak at 340 nm for both complexes **1a** and **2a**. Note that the lowest excited state mostly described by a HOMO to LUMO transition (94%) is calculated at 392 nm; however, this state cannot be isolated in the experimental spectrum due to its very small oscillator strength and is most likely merged with the tail of the lowest absorption band.

Even though there is a different ordering of the highest occupied levels between complexes **1a** and **2a**, see Table 2, we find a consistency in the electronic character of the states involved in each of the three energy regions, see Table 3. Note that state 9 in complex **2a** lies in between bands 2 and 3 but has been associated to band 2 due to the similarity of the electronic character. We describe hereafter in details the nature of the excited states in complex **1a**, pointing to the differences observed for **2a**.

Table 3 shows that the virtual orbitals involved in the dominant one-electron transitions are the LUMO, LUMO+1, and LUMO+2 for complex **1a** (LUMO and LUMO+1 for complex **2a**). The orbitals are strongly localized (more than 87%) on the dfppy ligands, thus confirming the key role played by these ligands. In the energy region around 250 nm (band 3), we find states with a dominant IL character involving either dfppy1 or dfppy2 as predicted but also states with dominant LMCT and LLCT contributions in complex **1a**. For the states in the energy region around 300 nm (band 2), the largest contributing character in the dominant transition is intraligand (IL) centered on dfppy1 for state 9 and on dfppy2 for state 15 in **1a**. Note that, for complex **2a**, there is also an important LLCT character in state 16, thus explaining the lower oscillator strength compared to state 11 exhibiting a dominant intra-ligand character. In the energy range between 305-340nm (band 1), there is a MLCT character involving dfppy1 in state 3 while the most important character in state 6 is IL targeted to dfppy2. Finally the dominant character of the lowest excited state (band 1') around 390 nm is linked to a charge transfer from Ir to dfppy2. However, there is also a small IL character that promotes a significant value for the

transition dipole moment since MLCT and LLCT transitions alone would give rise to very low values. We have further compared the relative intensities of the bands 1, 2, and 3 by plotting in Figure 5 the simulated spectra of the two complexes.[29] The calculated relative intensities of the three bands are consistent with the experimental spectra (40, 15, and 5 x 10^3 $M^{-1}cm^{-1}$ for bands 3, 2, and 1 to be compared with the calculated values of 30, 18, and 10 x 10^3 $M^{-1}cm^{-1}$ for complex **1a** and 25, 20, and 6 x 10^3 $M^{-1}cm^{-1}$ for complex **2a).**

Complexes **1** and **2** exhibit an intense blue emission with a 0-0 transition at ~ 452 nm in degassed CH_2Cl_2 solution and thin film (see Figure 6 and Table 4). All complexes show vibronically structured emission spectra at room temperature, indicating that the emissive excited states have a pronounced LC $\pi\pi^*$ character in addition to MLCT characters. Moreover, upon cooling the solution down to 77 K, the emission spectra of the complexes are much more structured and blue shifted (see Figure S2 to S5). The results unambiguously indicate that the lowest lying triplet excited state is a MLCT, as supported by the shift in energy of the emission upon cooling, with a pronounced $\pi\pi^*$ character. The spectral profile is reminiscent of other Ir(III) complexes having dfppy cyclometalated chelate and is comparable to that of cationic "blue-emitting" Ir(III) complexes with strongly π-accepting ligands.[7d,10a]

Table 5 describes the nature of the lowest triplet excited state of complexes **1a** and **2a** provided by TD-DFT calculations from the ground-state geometry in absence of spin-orbit coupling. The dominant character of the emitting state is MLCT with some admixture of LLCT and IL for **1a** and mostly MLCT for **2a**. The energy separation between the lowest singlet and triplet excited states is estimated by theory to be 0.32 and 0.30 eV for complexes **1a** and **2a** respectively. This value is smaller than the 0.70 eV estimated from the experimental data by subtracting the energy of the 0-0 peak of the lowest emission band (~ 2.74 eV) to the energy of the lowest intense absorption band (around ~ 3.44 eV) since the latter does not correspond to the lowest excited state. Moreover, the theoretical value is expected to be larger when accounting for the lattice relaxation effects in the triplet emitting state.

The absolute emission quantum yields of **1** ~ **2** measured by integrating sphere are in the range of Φ = 0.20 ~ 0.35 in degassed CH_2Cl_2 (see Table 4). We can observe that for the complexes containing the BF_4^- counter ion have quantum yield slightly higher than the corresponding complexes having the PF_6^- counterion. We have also measured the emission quantum yields of neat films and films with TBAOTf. The data show that the complexes with long *n*-butyl chain possess emission quantum yields double than those complexes containing the short methyl chains. This effect could be due to the fact that the long *n*-butyl chain prevents the stacking of the complexes reducing the quenching effect in the film, by decreasing the triplet-triplet annihilation. The excited state lifetimes of all the complexes investigated are in the range of 2.08 ~ 2.35 μs. The excited state lifetimes of complexes with BF_4^- counter ion are slightly longer than those of complexes with PF_6^- ion. From the quantum yield(Φ) and the lifetime(τ) values, assuming a unitary intersystem crossing efficiency, the radiative and overall non-radiative rate constants k_r and k_{nr} were calculated for using the equations $k_r = \Phi/\tau$ and $k_{nr} = (1 - \Phi)/\tau$ (see Table 4). [30]

Electrochemistry.

The electrochemical behavior of these Ir metal complexes was investigated by cyclic voltammetry using ferrocene as the internal standard. The results are summarized in Table 4. During the anodic scan in CH_3CN, all iridium metal complexes exhibited a reversible oxidation with potentials in the region of 0.97-1.05 V. Upon the switch to the cathodic sweep, two irreversible waves, with potentials ranging from -2.32 to -2.67 V, were detected. Since complexes **1** and **2** differ only by the nature of the terminal alkyl chain on the carbene ligand, their HOMO and LUMO levels and hence their redox potentials are expected to be similar. This is confirmed by the data in Table 2 showing that the HOMO is calculated at -5.95 eV and -5.83 eV for **1a** and **2a**, respectively while the LUMO stands at -2.06 eV and -1.95 eV, respectively. Therefore the oxidation is expected to occur primarily on the Ir metal site together with additional contributions from the cyclometalated dfppy ligands. On the other hand, the reduction process is concentrated on the pyridyl group of the dfppy chromophores.

Electroluminescence Properties: LEEC devices .

A schematic representation of the device architecture is shown in Figure 7. To investigate the electroluminescent properties of the devices based on the different complexes voltage sweeps, now referred to voltage sweep mode (VSM), to study the electric field stability range of the complexes as well as time dependent measurements at constant voltage, i.e. constant voltage mode (CVM), of the luminance and the current density were performed. In case of VSM the current density and the luminance were measured starting at 0 V (at time 0) and every 60 seconds the voltage was stepwise increased by 0.1 V until reaching 7.0 V. For CVM a constant voltage of U = 5.0 V was applied and the luminance was scanned every 10 seconds. Each curve is an average over 6 devices. As according to first experiments it turned out that the devices based on a neat film of complexes exhibited very long response times, the ionic conductor TBAOTf (Tetrabutylammonium trifluoromethanesulfonate) was added to the light emitting layer to make the turn-on faster. The molar ratio of Iridium complex and TBAOTf was set to 1:1 as this yielded the best device performance.

In Figure 8 typical device characteristics in VSM (Figure. 8a and 8b) and CVM (Figure. 8c and 8d) for **1a**, **1b**, **2a** and **2b** are shown. For all devices and for both operation modes a curve progression with a rising and a falling slope of the luminance was observed. For both modes the rising slope can be referred to decreasing injection barriers and a subsequently increase of injected charge carriers into the device. In the case of VSM such an injection enhancement is promoted by higher voltages due to a higher electrochemical potential difference between anode and cathode. For the CVM the increase in current and luminance is due to an increasing orientation of mobile ions along the external electrical field over time. The decay can be explained by device/complex instabilities at higher electric fields for VSM and time dependent device/complex degradation for CVM.

As shown the complexes including the short methyl chained biscarbene ligands (**1a** and **1b**, Lum ≈ 70 cd/m² and Lum ≈ 180 cd/m²) are more luminescent than the *n*-butyl long-chained ones (**2a** and **2b**, both

Lum ≈ 20 cd/m²) in VSM. However, such high differences of the maximum luminance between **1a/1b** and **2a/2b** are only observed for higher voltages U ≥ 6.0 V. In constant voltage mode at U = 5.0 V such diverse values are not significant, as the maximum luminance of **2a** is comparable with **1a/1b** for example. Best results in CVM in terms of device stability were achieved for the short chained carbene complex **1b** with BF_4^- counter ion. The time to reach the luminance maximum varies between 260s (**1a**) and 620s (**1b**). Interestingly, in both modes the luminance maximum does not match the maximum of the current density. Such a mismatch between current and light was also observed in former studies, e.g. for a $[Ir(ppy)_2(Hpbpy)][PF_6]$ complex reported by Bolink et al..[7d] In Figure 9 the current efficiency is depicted in VSM (Figure. 9a) and CVM (Figure. 9b). For both modes a comparable curve progression with a rising and a falling slope as for the luminance characteristic was observed whereas the efficiency maximum does not fit to the maximum of the luminance due to the mentioned mismatch between luminance and current density. The device characteristics of the devices based on the four iTMC complex strategies are summarized in Table 6.

Based on the cyclic voltammetry results shown in Table 4 with reversible oxidation from an anodic scan and irreversible reduction processes during the cathodic sweep of the complexes **1a**, **1b** and **2a**, **2b** in solution, it is expected that hole transport is more pronounced and stable than electron transport in a LEC configuration of these complexes. For a better charge balance and hence for a better LEC performance, especially with higher luminance and efficiency values, blending the complexes with more electron transporting materials could be a possible improvement.

In Figure 10, the electroluminescent (EL) emission spectra measured at fixed voltage of 5.5 V are shown. In particular, the complexes **2a** and **2b** exhibit blue to blue-green emission with local maxima at wavelengths of about λ_{max} 456 nm and 488 nm. The CIE coordinates value of complex **2a** is (0.20, 0.34). The CIE value of the device incorporating **2a** and ionic conductor indicate a substantially bluer emission than for other blue-phosphorescent dopants.[10a]

The spectrum of complex **2a** is comparable to the thin film PL spectra with 1:1 molar ratio (Figure S4). In contrast to that the EL spectra of the complexes **la** and **1b** were red-shifted with a peak at 488 nm compared to the PL spectra in solution and thin film with a peak at about 452-458 nm (Figure S2~S5). This similar red-shifted phenomenon for blue-emitting Iridium LEECs has also been observed in a recent paper.[31] We believe that the longer alkyl chains in compounds **2** prevent aggregation which is responsible for the red shift of the complexes **1**. This finding could help the design of the next generation of blue LEECs.

Conclusions

Four novel blue-emitting cationic iridium complexes have been synthesized and fully characterized. We have designed and used two types of biscarbene as ancillary ligand differing for the length of the alkyl chain attached to the nitrogen atoms. We have prepared the corresponding cationic Iridium complexes isolating them using different counterions. Theoretical calculations address almost no difference between the two types of ancillary ligands for which the HOMO consists on a mixture between the Ir and difluorophenyl pyridine species and the LUMO is mostly located on the other difluorophenyl pyridine ligand. The importance of ^{3}LC character in the emissive states is confirmed by the theoretical calculations. These Ir complexes exhibit efficient blue emission in solution and thin film. The LEEC devices made using the Iridium (III) carbene-typed complex and a new ionic conductor (TBATOf) have short devices turn on time (few seconds) and exhibit blue emission. Our molecular-design strategy based on using high ligand-field carbene ligands suggests that the emission of iTMCs can be efficiently tuned to blue or deep blue region.

Acknowledgments

The authors would like to thank *Siemens AG, Corporate Technology, CT MM 1* and the European Community Seventh Framework Programme (FP7/2007-2013) under grant agreement n° 212311 of the ONE-P project for financial support. Dr. Cheng-Han Yang would like to acknowledge the Humboldt Foundation for financial support. The work in Mons is also supported by the Belgian National Fund for Scientific Research (FNRS). This research used resources of the Interuniversity Scientific Computing Facility located at the University of Namur, Belgium, which is supported by the F.R.S.-FNRS under convention No. 2.4617.07. J.C. is a senior research associate of FNRS.

Supporting Information Available:

X-ray crystallographic data file (CIF) for complexes **1a** and **2a**. ORTEP diagram of **1a** and crystal data and structure refinement parameters for complexes **1a** and **2a.** Emission spectra of complexes **1a, 1b, 2a** and **2b.** Comparison between theory and experiment for the representative distances and bond angles for complexes **1a** and **2a.** Electronic structure of complex **1a** in absence or in presence of the counter-ion. This material is available free of charge via the Internet at http://pubs.acs.org.

Figure Captions:

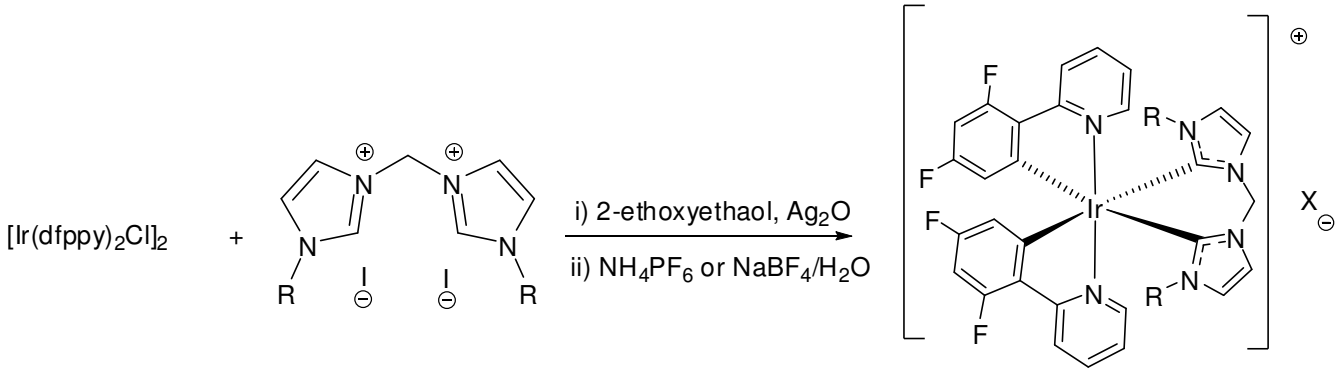

R = CH_3 1a (X= PF_6)
1b (X=BF_4)

R = C_4H_9 2a (X=PF_6)
2b (X=BF_4)

Scheme 1. Synthetic pathways and chemical structures and abbreviations of the investigated complexes

Table 1. Selected bond length (Å) and angles (°) for complex **1a** and **2a**

Complex **1a·PF_6·CH_3CN**			
Ir–$C_{carbene}$(1)	2.112(5)	Ir–$C_{carbene}$ (11)	2.114(5)
Ir–N(21)	2.053(4)	Ir–C(32)	2.063(4)
Ir–N(41)	2.052(4)	Ir–C(52)	2.043(4)
C(1)–Ir–C(32)	173.22(17)	C(52)–Ir–C(11)	172.74(18)
N(21)–Ir–N(41)	169.39(16)	C(32)–Ir–N(21)	79.19(17)
C(52)–Ir–N(41)	79.65(17)	C(1)–Ir–C(11)	85.82(18)
Complex **2a·PF_6·CH_3CN**			
Ir–$C_{carbene}$(2)	2.120(1)	Ir–$C_{carbene}$ (12)	2.104(1)
Ir–N(21)	2.055(1)	Ir–C(32)	2.054(1)
Ir–N(41)	2.072(1)	Ir–C(52)	2.054(1)
C(2)–Ir–C(32)	173.58(14)	C(52)–Ir–C(12)	174.94(12)
N(21)–Ir–N(41)	170.77(12)	C(32)–Ir–N(21)	80.00(14)
C(52)–Ir–N(41)	79.20(14)	C(2)–Ir–C(12)	85.28(15)

Table 2. Energies and contribution (in %) of the different fragments for the frontier electronic levels ranging from HOMO-5 to LUMO+5 for complex **1a** (left) and **2a** (right), which are referred as H-5 and L+5 in the table.

FO	Energy	Ir	methyl	dfppy1	dfppy2	Energy	Ir	butyl	dfppy1	dfppy2
H-5	-6.72	4	16	34	46	-6.66	5	13	14	67
H-4	-6.61	42	15	23	19	-6.49	6	19	30	45
H-3	-6.50	20	15	23	41	-6.29	45	21	14	19
H-2	-6.45	45	21	9	24	-6.23	15	14	48	22
H-1	-6.30	16	9	60	15	-6.20	42	26	24	8
H	**-5.95**	**43**	**11**	**31**	**16**	**-5.83**	**43**	**13**	**32**	**12**
L	**-2.06**	**5**	**3**	**3**	**90**	**-1.95**	**4**	**5**	**2**	**88**
L+1	-1.59	5	5	87	3	-1.55	4	4	86	5
L+2	-1.55	4	5	2	89	-1.41	3	4	4	89
L+3	-0.96	5	5	88	3	-0.88	3	6	86	4
L+4	-0.53	14	69	6	11	-0.28	18	46	10	26
L+5	-0.19	7	46	41	6	-0.06	9	27	4	59

Table 3. Characterization of the most optically-coupled lowest singlet excited states (ES); we provide the nature of the dominant one-electron transition from a given occupied (Occ) to unoccupied (Vir) level including the contribution in percents as well as the oscillator strength (f) and energy of the states both in eV and nm. The second most important character has been included only when its weight is larger than 2/3 of the most important one. The weight of the characters in percents is included between parentheses.

1a	**ES**	**Occ**	**Vir**	**eV/nm**	**f**	**%**	**Character**
Band 1'	1	**H**	**L**	3.16/393	0.01	94	MLCT (40%),LLCT(30%)
Band 1	3	**H**	L+1	3.63/341	0.03	89	MLCT
	6	H-3	**L**	3.81/325	0.06	25	IL
Band 2	9	H-1	L+1	4.09/302	0.05	50	IL
	15	H-3	L+2	4.33/286	0.05	36	IL
Band 3	22	H-6	**L**	4.69/264	0.17	37	LMCT(30%), LLCT(23%)
	24	H-1	L+3	4,79/259	0.10	48	IL
2a	**ES**	**Occ**	**Vir**	**eV/nm**	**f**	**%**	**Character**
Band 1'	1	H	**L**	3.16/392	0.01	94	MLCT(40%) ,LLCT(30%)
Band 1	4	H-3	**L**	3.62/343	0.03	73	MLCT
	7	H-4	**L**	3.92/316	0.03	77	IL(40%), LLCT(30%)
	9	H-3	L+1	4.03/307	0.05	52	MLCT
Band 2	11	H-2	L+1	4.15/299	0.08	40	IL
	16	H-4	L+1	4.37/284	0.05	59	LLCT(40%) ,IL(30%)
Band 3	22	H-5	L+2	4.69/264	0.07	45	IL
	30	H-2	L+3	4.95/251	0.12	28	IL

Table 4. Photophysical and Electrochemical data of Iridium complexes

	Em.λ/nm[a], Φ_{sol}[d]	λ_{film}/nm[b], Φ_{film}[d]	λ_{film} /nm[c], Φ_{film}[d]	τ_{obs} / μs	k_r ($10^5 s^{-1}$)	k_{nr} ($10^5 s^{-1}$)	E_{ox} [v][e]	E_{re} [v][e]
1a(PF_6)	452,482 [0.20]	460,484 [0.02]	457,484 [0.07]	2.08	0.96	3.8	0.99	-2.32; -2.67
1b(BF_4)	452,480 [0.30]	458,484 [0.03]	457,484 [0.07]	2.33	1.28	3.0	0.97	-2.39; -2.67
2a(PF_6)	452, 482 [0.26]	458,484 [0.06]	455,483 [0.14]	2.21	1.18	3.35	1.04	-2.38, -2.67
2b(BF_4)	452, 480 [0.35]	458,484 [0.06]	454,482 [0.13]	2.35	1.49	2.77	1.05	-2.37, -2.67

[a] Degassed CH_2Cl_2 solution (298 K) [b] Neat Film [c] Film containing TBAOTf (1:1 molar ratio)

[d] PL QYs were determined with a calibrated Integrating sphere system

[e] Electrochemical data versus Fc^+/Fc (Fc is ferrocene) were collected in MeCN

Table 5. Characterization of the first triplet excited state at the TD-DFT level in the absence of spin-orbit coupling; we provide the same parameters as in Table 3 together with the energy separation between S_1 and T_1, as obtained from the ground-state geometry.

	Occ	**Vir**	**eV/nm**	**%**	**Character**	**S_1-T_1(eV)**
1a	**H**	**L**	2.84/436	46	MLCT(43%), LLCT(31%)	0.32
	H-3	**L**		15	IL	
2a	**H**	**L**	2.86/434	34	MLCT(43%),LLCT(32%),	0.30
	H-3	**L**		21	MLCT	

Table 6. Summary of the device characteristic based on Complexes **1a** to **2b**

Complex	t_{max}[a] [min]	L_{max}[b] [cdm^{-2}]	L_{max}[c] [cdm^{-2}]	Eff.[d] [cd/A]	Eff.[e] [cd/A]	$\lambda_{max,EL}$[f] [nm]	Lifetime [g] [min]	CIE (x,y)[h]
1a	4.5	69.8	21.6	0.46	0.73	488	8.0	0.27,0.43
1b	10.6	159.8	25.7	0.29	0.50	488	53.8	0.27,0.43
2a	5.3	17.2	24.0	0.89	0.37	456,488	9.8	0.20,0.34
2b	7.8	23.8	13.4	0.49	0.85	456,488	16.7	0.22,0.38

[a] Time required to reach the maximal brightness in CVM. [b] Maxima brightness achieved in VSM. [c] Maxima brightness achieved at a constant bias voltage 5.0 V (CVM). [d] Maximum current efficiency in VSM [e] Maximum current efficiency in CVM. [f] EL peak wavelength measured at 5.5 V. [g] Time to decay to the half of the maximum luminance under a constant bias voltage of 5.0 V (CVM). [h] CIE evaluated from the EL spectra.

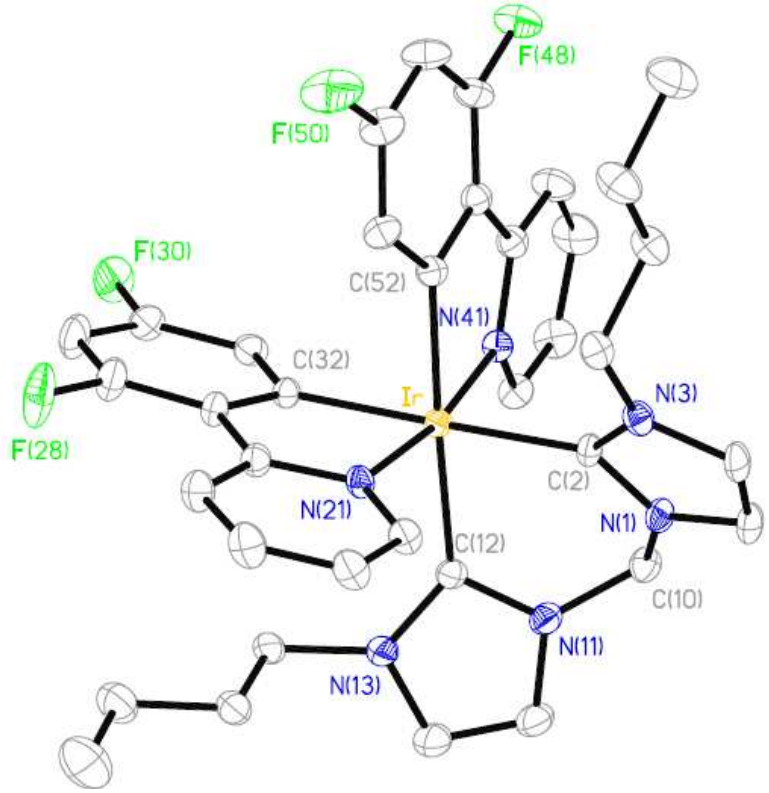

Figure 1. ORTEP diagram of **2a** with thermal ellipsoids shown at 30% probability level. The CH_3CN solvent molecules, counter anions (PF_6^-), and hydrogen atoms are omitted for clarity.

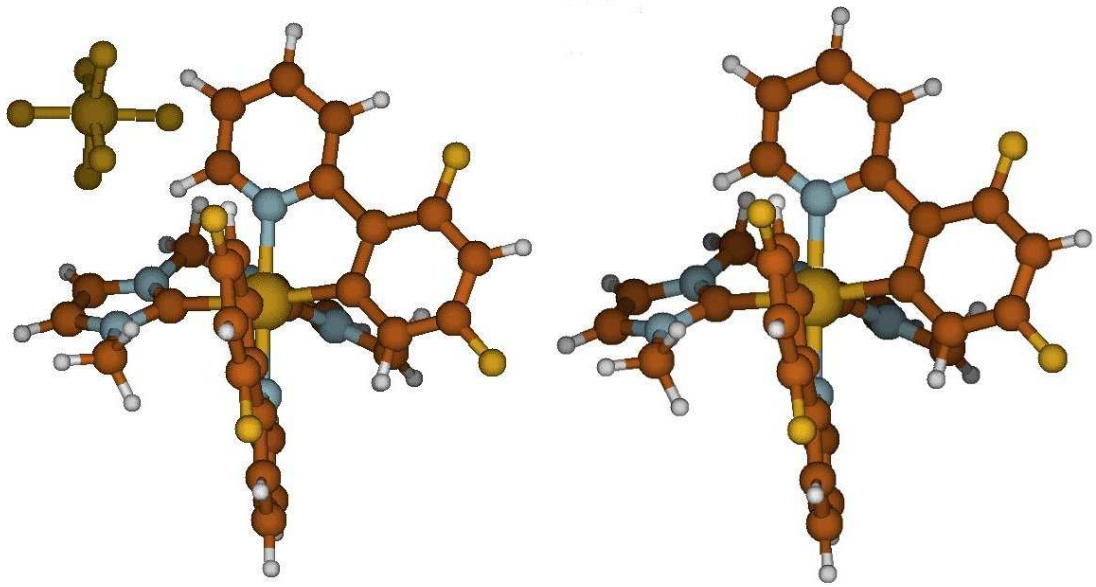

Figure 2. Calculated molecular geometries of the complex **1a** with (left) and without (right) the counter-ion.

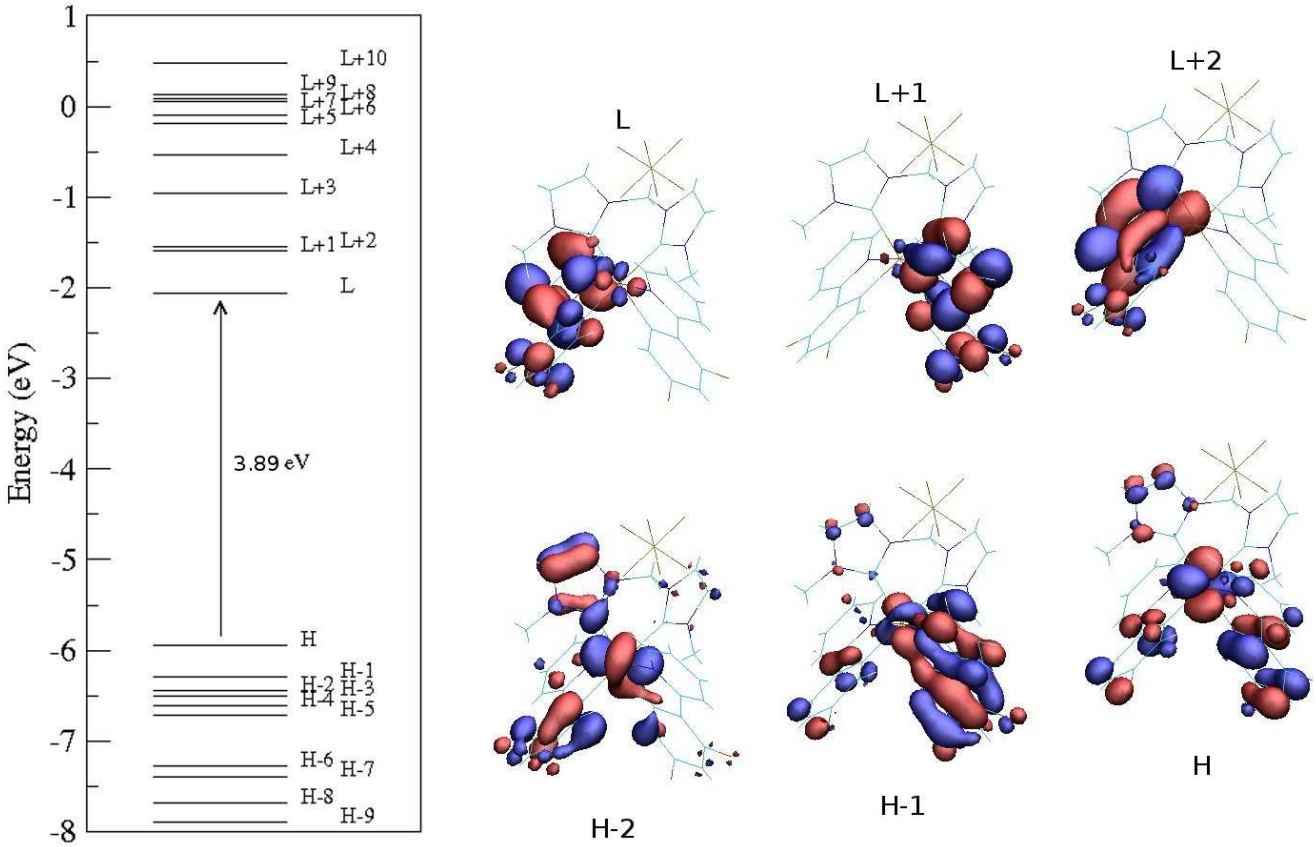

Figure 3. Electronic structure and shape of the frontier electronic levels from HOMO-2 to LUMO+2, referred as H-2 and L-2 respectively, of complex **1a**.

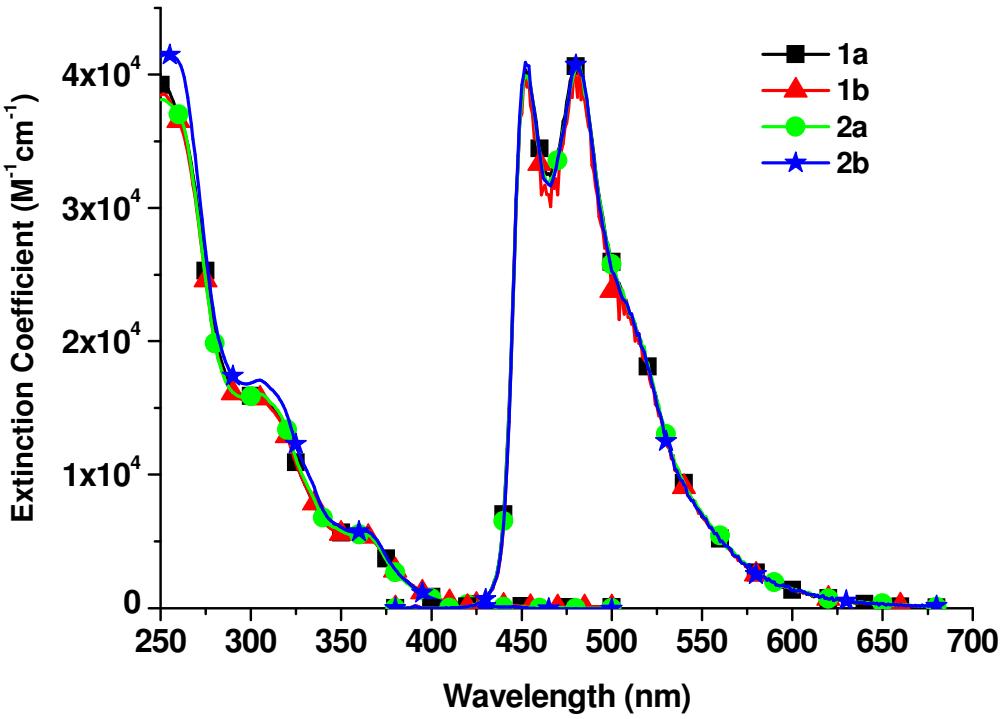

Figure 4. Absorption and PL spectra in DCM solution at RT

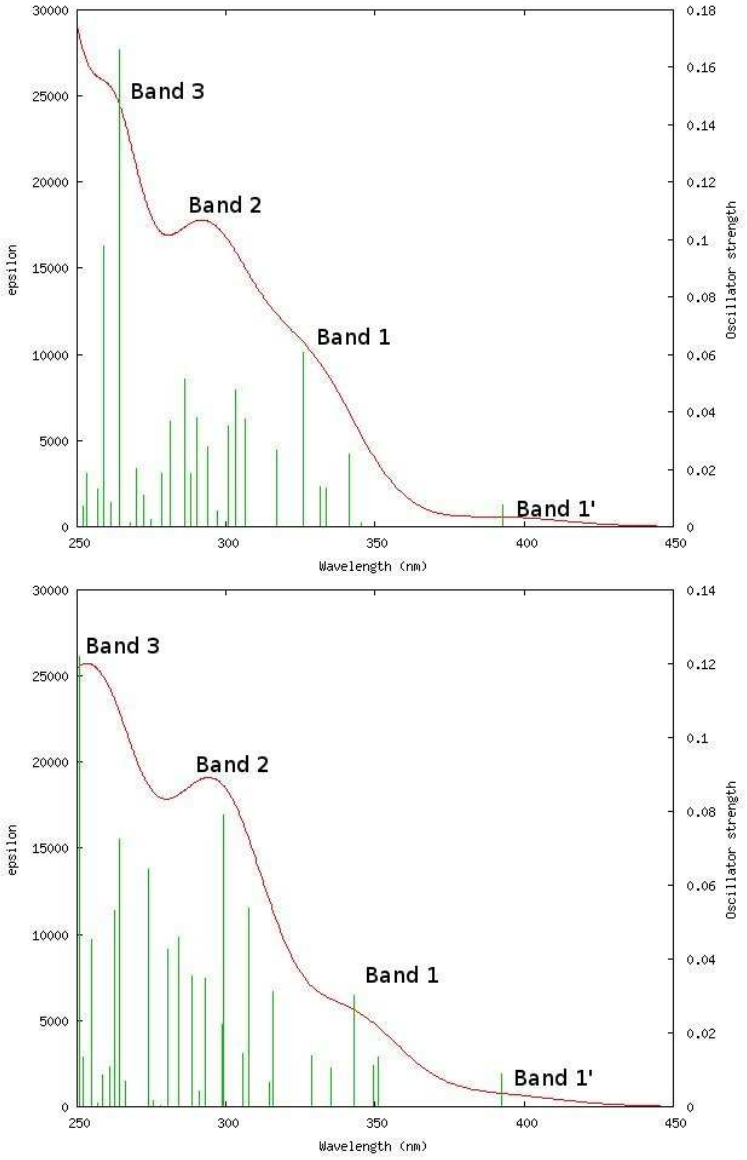

Figure 5. TD-DFT simulated absorption spectra of complex **1a** (up) and **2a** (down) using a full width at half maximum of 3000 cm^{-1}. The vertical bars correspond to the individual excited states.

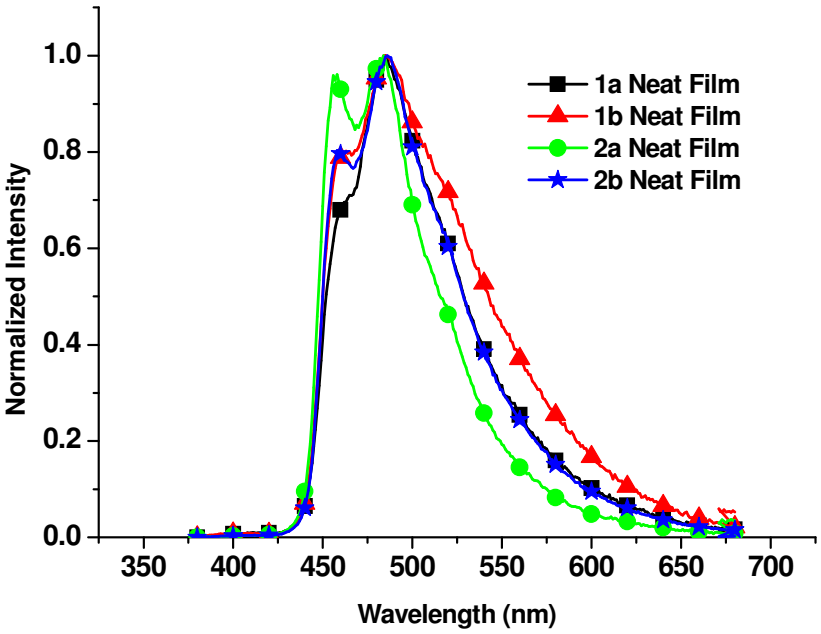

Figure 6. Emission spectra of Iridium complexes in Neat Film

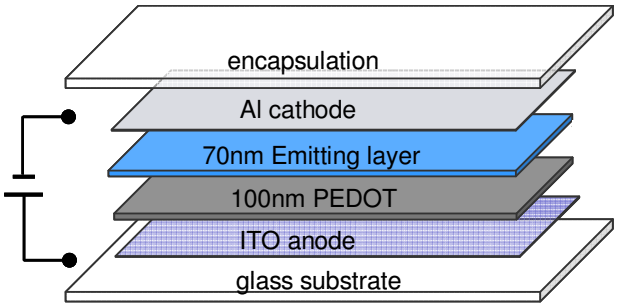

Figure 7. Schematic view of the device structure.

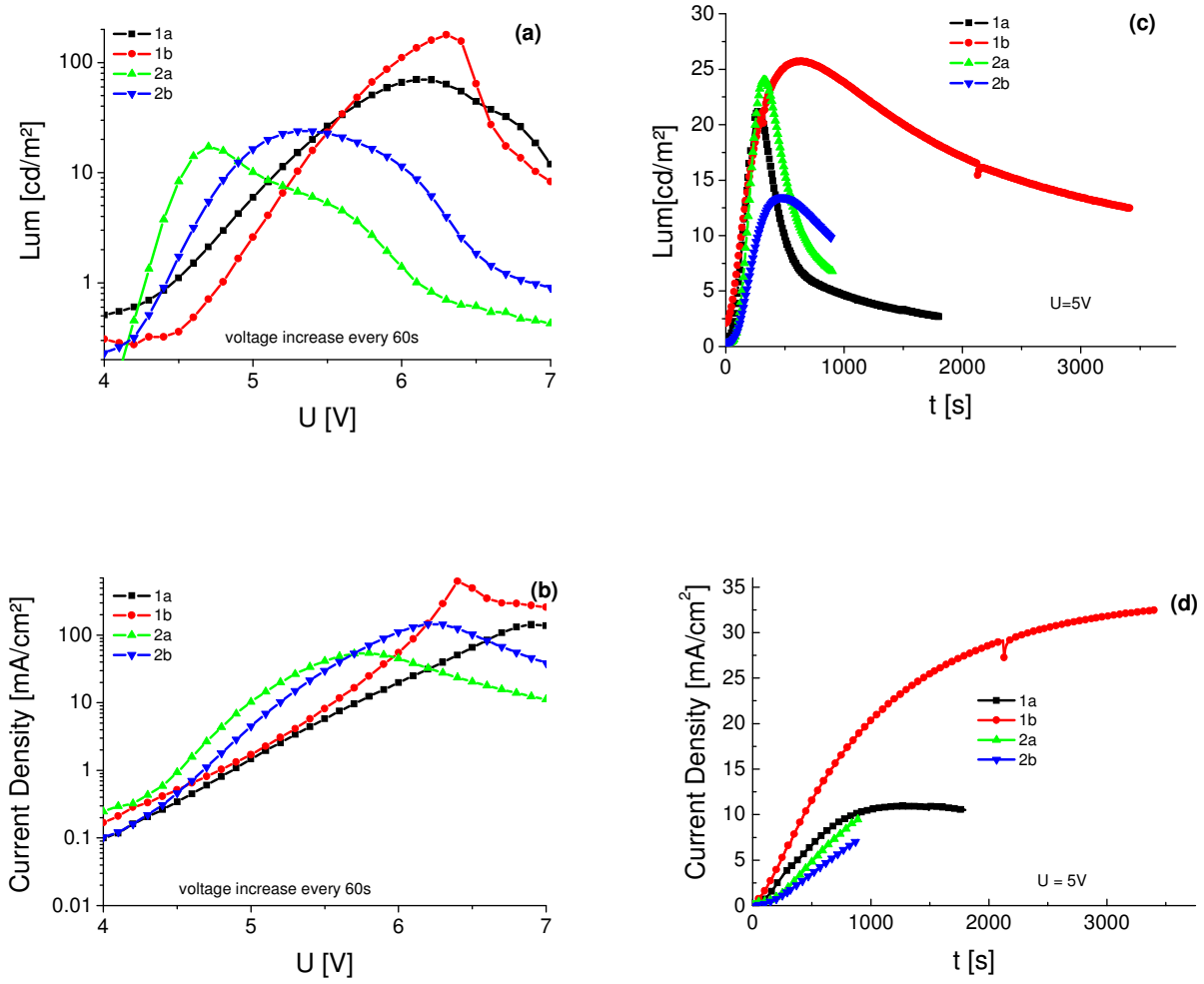

Figure 8. Voltage versus luminance (a) and voltage versus current density (b) curves under voltage sweep mode (VSM); Time-dependent luminance (c) and time-dependent current-density curves under constant voltage mode (CVM).

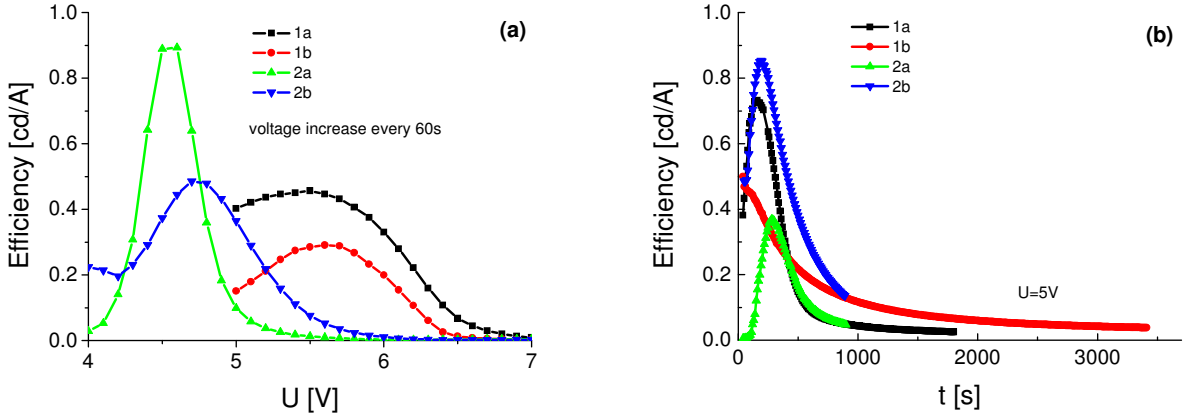

Figure 9. (a) Voltage versus current efficiency under voltage sweep mode (VSM) (b) time-dependent current efficiency curves under constant voltage mode (CVM).

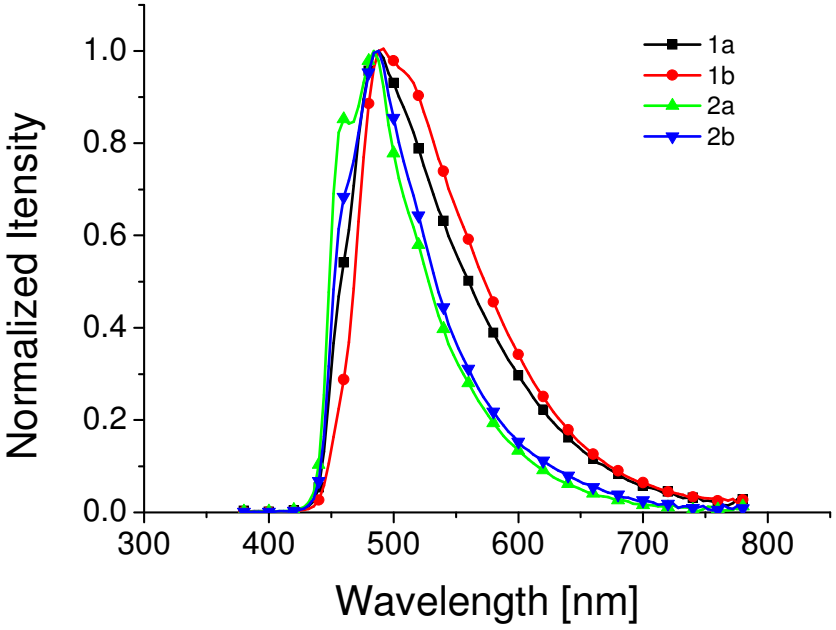

Figure 10. Electroluminescent spectra for LEEC devices.

Table of Contents synopsis

Blue emissive light-emitting electrochemical cells have been prepared based on heteroleptic Ir(III)-complexes containing N-heterocyclic carbenes as ancillary ligands.

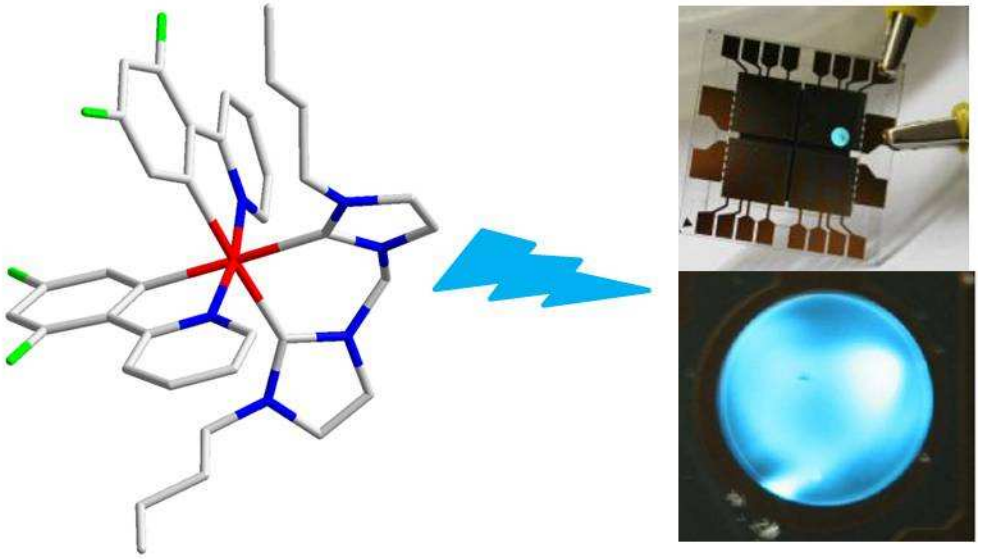

[1] a) Welter, S.; Brunner, K.; Hofstraat, J. W.; De Cola, L. *Nature* **2003**, *421*, 54 b) Slinker, J. D.; Rivnay, J.; Moskowitz, J. S.; Parker, J. B.; Bernhard, S.; Abruna, H. D.; Malliaras, G. G. *J. Mater. Chem.* **2007**, 17, 2976, c) Slinker, J. D.; Bernards, D.; Houston, P. L.; Abruña, H. D.; Bernhard, S.; Malliaras, G. G. *Chem. Commun.* **2003**, 2392.

[2] Slinker, J. D.; Defranco, J. A.; Jaqutth, M. J.; Silveir, W. R.; Zhong, Y. W.; Moran-Mirabal, J. M.; Craighead, H. G.; Abruña, H. D.; Marohn, J. A.; Malliaras, G. G. *Nat. Mater.* **2007**, *6*, 894.

[3] a) Lyons, C. H.; Abbas, E. D.; Lee, J.-K.; Rubner, M. F. *J. Am. Chem. Soc.* **1998**, *120*, 12100. b) Gao, F. G.; Bard, A. J. *J. Am. Chem. Soc.* **2000**, *122,* 7426. c) Buda, M.; Kalyuzhny, G.; Bard, A. J. *J. Am. Chem. Soc.* **2002**, *124*, 60908.

[4] a) Gao, F. G.; Bard, A. J. *Chem. Mater.* **2002**, *14*, 3465. b) Bernhard, S.; Gao, X. C.; Malliaras, G. G.; Abruña, H. D. *Adv. Mater.* **2002**, *14*, 433. c) Hosseini, A. R.; Koh, C. Y.; Slinker, J. D.; Torres, S. F.; Abruña, H. D.; Malliaras, G. G. *Chem. Mater.* **2005**, *17*, 6114.

[5] a) Zhang, Q. S.; Zhou, Q. G.; Cheng, Y. X.; Wang, L. X.; Ma, D. G.; Jing, X. B.; Wang, F. S. *Adv. Funct. Mater.* **2006**, *16*, 1203. b) Armaroli, N.; Accorsi, G.; Michel, H., Moudam, O.; Nierengarten, J. F.; Zhou, Z.; Wegh, R. T.; Welter, R. *Adv. Mater.* **2006**, *18*, 1313. c) Zhang, Q. S.; Zhou, Q. G.; Cheng, Y. X.; Wang, L. X.; Ma, D. G.; Jing, X. B.; Wang, F. S. *Adv. Mater.* **2004**, *16*, 432. d) Wang, Y. M.; Teng, F. Y.; Hou, B.; Xu, Z.; Wang, Y. S.; Fu, W. F. *Appl. Phys. Lett.* **2005**, *87*, 233512.

[6] a) Slinker, J. D.; Gorodetsky, A. A.; Lowry, M. S.; Wang, J. J.; Parker, S.; Rohl, R.; Bernhard, S.; Malliaras, G. G. *J. Am. Chem. Soc.* **2004**, *126*, 2763. b) Slinker, J. D.; Koh, C. Y.; Malliarasa, G. G.; Lowry, M. S.; Bernhard, S. *Appl. Phys. Lett.* **2005**, *86*, 173506. c) Lowry, M. S.; Goldsmith, J. I.; Slinker, J. D.; Rohl, R.; Pascal, R.; Jr, A.; Malliaras, G. G.; Bernhard, S. *Chem. Mater.* **2005**, *17*, 5712. d) Tamayo, A. B.; Garon, S.; Sajoto, T.; Djurovich, P. I.; Tsyba, I. M.; Bau, R.; Thompson, M. E. *Inorg. Chem.* **2005**, *44*, 8723. e) Nazeeruddin, M. K.; Wegh, R. T.; Zhou, Z.; Klein, C.; Wang, Q.;

Angelis, F. D.; Fantacci, S.; Grätzel, M. *Inorg. Chem.* **2006**, *45*, 9245. f) Bolink, H. J.; Coronado, E.; Costa, R. D.; Lardiés, N.; Ortí, E. *Inorg. Chem.* **2008**, *47*, 9149.

[7] a) Bolink, H. J.; Cappelli, L.; Coronado, E.; Parham, A.; Stössel, P. *Chem. Mater.* **2006**, *18*, 2778. b) Su, H. -C.; Wu, C. -C.; Fang, F. -C.; Wong, K. -T. *Appl. Phys. Lett.* **2006**, *89*, 261118. c) Bolink, H. J.; Cappelli, L.; Coronado, E.; Grätzel, M.; Ortí, E.; Costa, R. D.; Viruela, P. M.; Nazeeruddin, M. K. *J. Am. Chem. Soc.* **2006**, *128*, 14786. d) Bolink, H. J.; Coronado, E.; Costa, R. D.; Ortí, E.; Sessolo, M.; Graber, S.; Doyle, K.; Neuburger, M.; Housecroft, C. E.; Constable, E. C. *Adv. Mater.* **2008**, *20*, 3910. e) Kwon, T. H.; Oh, Y. H.; Shin, I. S.; Hong, J. I. *Adv. Funct. Mater.* **2009**, *19*, 711.

[8] a) Su, H. -C.; Fang, F.- C.; Hwu, T. -Y.; Hsieh, H. -H.; Chen, H. -F.; Lee, G. -H.; Peng, S. -M.; Wong, K. -T.; Wu, C. -C. *Adv. Funct. Mater.* **2007**, *17*, 1019. b) Colman, E. Z.; Slinker, J. D.; Parker; J. B.; Malliaras, G. G.; Bernhard, S. *Chem. Mater.* **2008**, *20*, 388. c) Graber, S.; Doyle, K.; Neuburger, M.; Housecroft, C. E.; Constable, E. C.; Costa, R. D.; Ortí, E.; Repetto, D.; Bolink, H. J. *J. Am. Chem. Soc.* **2008**, *130*, 14944.

[9] a) Su, H. -C.; Chen, H. -F.; Fang, F. -C.; Liu, C. -C.; Wu, C. -C.; Wong, K. -T.; Liu, Y. -H.; Peng, S. -M. *J. Am. Chem. Soc.* **2008**, *130*, 3414. b) He, L.; Qiao, J.; Duan, L.; Dong, G.; Zhang, D.; Wang, L.; Qiu, Y. *Adv. Funct. Mater.* **2009**, *19*, 2950.

[10] a) He, L.; Duan, L.; Qiao, J.; Wang, R.; Wei, P.; Wang, L.; Qiu, Y. *Adv. Funct. Mater.* **2008**, *18*, 2123. b) Unger, Y.; Zeller, A.; Ahrens, S.; Strassner, T. *Chem. Commun*., **2008**, 3263. c) Lowry, M. S.; Bernhard, S. *Chem. Eur. J*. **2006,** *12*, 7970. d) Unger, Y.; Zeller, A.; Taige, M. A. Strassner, T. *Dalton Trans.,* **2009***,* 4786.

[11] (a) Yang, C.-H.; Li, S.-W.; Chi, Y.; Cheng, Y.-M.; Yeh, Y.-S.; Chou, P.-T.; Lee, G.-H.; Wang, C.-H.; Shu, C.-F. *Inorg. Chem.* **2005**, *44*, 7770. b) Yang, C.-H.; Cheng, Y.-M.; Chi, Y.; Hsu, C.-J.; Fang, F.-C.; Wong, K.-T.; Chou, P.-T.; Chang, C.-H.; Tsai, M.-H.; Wu, C.-C. *Angew. Chem. Int. Ed.* **2007**, *46*, 2418. c) Sajoto, T.; Djurovich, P. I.; Tamayo, A. B.; Oxgaard, J.; Goddard, W. A.; Thompson, M. E. *J. Am. Chem. Soc.* **2008**, *131*, 9813.

[12] a) Li, J.; Djurovich, P. I.; Alleyne, B. D.; Yousufuddin, M.; Ho, N. N.; Thomas, J. C.; Peters, J. C.; Bau, R.; Thompson, M. E. *Inorg.Chem.* **2005**, *44*,1713. b) Chang, C.-F.; Cheng, Y.-M.; Chi, Y.; Chiu, Y.-C.; Lin, C.-C.; Lee, G.-H.; Chou, P.-T.; Chen, C.-C; Chang, C.-H.; Wu, C.-C. *Angew. Chem. Int. Ed.* **2008**, *120*, 4618. c) Chi, Y., Chou, P.-T. *Chem. Soc. Rev.*, **2010**, *39*, 638

[13] Nonoyama, M. *Bull. Chem. Soc. Jpn.* **1974**, *47*, 767.

[14] Nonius, B.V., 1998.

[15] Otwinowski, Z., Minor, W. *Macromolecular Crystallography, Part A,* Academic Press Inc, San Diego, **1997**, *276*, 307.

[16] Blessing, R. H. *Acta Crystallogr., Sect. A,* **1995**, *51*, 33.

[17] Blessing, R. H., *J. Appl. Crystallogr.*, **1997**, *30*, 421.

[18] Otwinowski, Z.; Borek, D.; Majewski, W.; Minor, W. *Acta Crystallogr., Sect. A,* **2003**, *59*, 228.

[19] Sheldrick, G. M. *Acta Crystallogr., Sect. A*, **1990**, *46*, 467.

[20] Sheldrick, G. M. Universität Göttingen, Göttingen, Germany, **1997**

[21] Keller, E. Universität Freiburg, **1997**.

[22] a) Lee, C. T.; Yang, W. T.; Parr, R. G. *Phys. Rev. B*, **1988**, *37*, 785. b) Becke, A. D. *J. Chem. Phys.,* **1993**, *98*, 5648.

[23] Curtiss, L. A.; Redfern, P. C.; Raghavachari, K.; Pople, J. A. *J. Chem. Phys.,* **2001***, 114*, 108.

[24] Chiodo, S.; Russo,N.; Sicilia, E. *J. Chem. Phys.,* **2006**, *125*, 104107.

[25] Avilov, I.; Minoofar, P.; Cornil, J.; De Cola, L. *J. Am. Chem. Soc.*, **2007**, *129*, 8247.

[26] Vlcek, A.; Zalis, S. *Coordin. Chem. Rev.*, **2007**, *251*, 258.

[27] Gaussian 03, Revision C.02, Frisch, M. J.; Trucks, G. W.; Schlegel, H. B.; Scuseria, G. E.; Robb, M. A.; Cheeseman, J. R.; Montgomery, Jr., J. A.; Vreven, T.; Kudin, K. N.; Burant, J. C.; Millam, J. M.; Iyengar, S. S.; Tomasi, J.; Barone, V.; Mennucci, B.; Cossi, M.; Scalmani, G.; Rega, N.; Petersson, G. A.; Nakatsuji, H.; Hada, M.; Ehara, M.; Toyota, K.; Fukuda, R.; Hasegawa, J.; Ishida, M.; Nakajima, T.; Honda, Y.; Kitao, O.; Nakai, H.; Klene, M.; Li, X.; Knox, J. E.; Hratchian, H. P.; Cross, J. B.;

Bakken, V.; Adamo, C.; Jaramillo, J.; Gomperts, R.; Stratmann, R. E.; Yazyev, O.; Austin, A. J.; Cammi, R.; Pomelli, C.; Ochterski, J. W.; Ayala, P. Y.; Morokuma, K.; Voth, G. A.; Salvador, P.; Dannenberg, J. J.; Zakrzewski, V. G.; Dapprich, S.; Daniels, A. D.; Strain, M. C.; Farkas, O.; Malick, D. K.; Rabuck, A. D.; Raghavachari, K.; Foresman, J. B.; Ortiz, J. V.; Cui, Q.; Baboul, A. G.; Clifford, S.; Cioslowski, J.; Stefanov, B. B.; Liu, G.; Liashenko, A.; Piskorz, P.; Komaromi, I.; Martin, R. L.; Fox, D. J.; Keith, T.; Al-Laham, M. A.; Peng, C. Y.; Nanayakkara, A.; Challacombe, M.; Gill, P. M. W.; Johnson, B.; Chen, W.; Wong, M. W.; Gonzalez, C.; and Pople, J. A.; *Gaussian, Inc.*, Wallingford CT, **2004**.

[28] a) Coppo, P.; Plummer, E. A.; De Cola, L. *Chem. Commun.*, **2004**, 1774. b) Orselli, E.; Kottas, G. S.; Konradsson, A. E.; Coppo, P.; Fröhlich, R.; De Cola, L.; VanDijken, A.; Büchel, M.; Börner, H. *Inorg. Chem.*, **2007**, *46*, 11082. c) Orselli, E.; Albuquerque, R. Q.; Michel Fransen, P.; Fröhlich, R. Janssenc, H. M.; De Cola, L. *J. Mater. Chem.* **2008**, *18*, 4579.

[29] O'Boyle, N. M.; Tenderholt, A. L.; Langner, K. M. *J. Comp. Chem.*, **2008**, *29*, 839.

[30] Kober, E. M.; Caspar, J. V.; Lumpkin, R. S.; Meyer, T. J. *J. Phys. Chem.* **1986**, *90*, 3722.

[31] a) Bolink, H. J.; Cappelli, L.; Cheylan, S.; Coronado, E.; Costa, R. D.; Lardiés, N.; Nazeeruddin, M. K.; Ortí, E. *J. Mater. Chem.* **2007**, *17*, 5032. b) Margapoti, E.; Shukla, V.; Valore, A.; Sharma, A.; Dragonetti, C.; Kitts, C. C.; Roberto, D.; Murgia, M.; Ugo, R.; Muccin, M. *J. Phys. Chem. C*, **2009**, *113*, 12517.